

<https://doi.org/10.1038/s42003-025-07458-5>

# A perfusion-independent high-throughput method to isolate liver sinusoidal endothelial cells

Check for updates

Anna Babin-Ebell Gonçalves<sup>1,2,13</sup>, Yifang Mao<sup>1,3,13</sup>, Tinja Baljkas<sup>4,5,13</sup>, Felix Wiedmann<sup>6,7</sup>, Larissa Eis<sup>8</sup>, Franziska Pilz<sup>1</sup>, Manuel Winkler<sup>4,5</sup>, Sina W. Kürschner-Zacharias<sup>4,5</sup>, Marlene Hoffarth<sup>1,9</sup>, Charlotta Funaya<sup>8</sup>, Réza Shahidi<sup>8</sup>, Cyrill Géraud<sup>4,10,11</sup>, Chi-Chung Wu<sup>9,12</sup>, Constanze Schmidt<sup>6,7,9</sup>, Sergij Goerdts<sup>4,5</sup>, Philipp-Sebastian Reiners-Koch<sup>4,5</sup> & Mahak Singhal<sup>1,7,9</sup> ✉

Liver sinusoidal endothelial cells (LSECs) critically regulate homeostatic liver function and liver pathogenesis. However, the isolation of LSECs remains a major technological bottleneck in studying molecular mechanisms governing LSEC functions. Current techniques to isolate LSECs, relying on perfusion-dependent liver digestion, are cumbersome with limited throughput. We here describe a perfusion-independent high-throughput procedure to isolate LSECs with high purity. Indifferently from previous perfusion-independent approaches, chopped liver tissue was incubated in the digestion mix for 30 minutes with intermittent mixing with a serological pipette. This led to the safeguarding of LSEC integrity and yielded  $10 \pm 1.0$  million LSECs per adult mouse liver, which is far higher than previous perfusion-independent protocols and comparable yield to established perfusion-dependent protocols for isolating LSECs. Combining magnetic and fluorescence-activated cell sorting (FACS), LSECs from different zones of the hepatic sinusoid can now be isolated in high numbers in less than two hours for downstream applications including proteomics. Our protocol enables the isolation of LSECs from fibrotic liver tissues from mice and healthy liver tissues from higher vertebrate species (pigs), where traditional perfusion-based digestion protocols have very limited application. In conclusion, these technical advancements reduce post-mortem changes in the LSEC state and aid in reliable investigation of LSEC functions.

The liver is the metabolic powerhouse of our body. While hepatocytes serve as key functional units of the liver driving major metabolic processes, LSECs have emerged as critical modulators of hepatic function in the past decade<sup>1</sup>. LSECs are anatomically unique as they lack an organized basement membrane and harbor fenestrae to facilitate macromolecular transport to and from hepatocytes<sup>2,3</sup>. Further, LSECs secrete angiocrine signals to orchestrate hepatocyte functional zonation. In line, genetic ablation of Rspodin 3, a canonical Wnt activator primarily derived from LSECs, disrupted the metabolic zonation of hepatocytes along a liver sinusoid in adult mice<sup>4</sup>. Likewise, angiocrine signals Wnt2 and Wnt9b regulate the expansion of Axin2+ hepatocytes to maintain hepatocyte turnover under homeostatic conditions<sup>5,6</sup>. Additionally, recent evidence suggests an age-related decline in LSEC function predisposes the liver towards a higher risk of developing steatosis<sup>7</sup>. Together, these studies highlight the gatekeeper functions of LSECs in maintaining

liver health. Yet, these new findings have raised more questions about the functionality of LSECs and how can angiocrine signals be exploited as potential therapeutic targets to ameliorate liver pathologies.

Attributed to the discontinuous structure of sinusoidal vasculature, the isolation of healthy LSECs has been a challenging bottleneck for pursuing *ex vivo* functional analysis. Numerous LSEC isolation procedures have been described with the majority of those employing perfusion of the liver with tissue digestion buffer followed by a combination of magnetic and FACS-based enrichment of LSECs<sup>8</sup>. While perfusing the liver with digestion buffer allows isolating LSECs, it poses three major challenges—(i) perfusing *per se* applies mechanical shear that potentially induces molecular alterations in LSECs' gene circuits, (ii) it strongly limits the throughput as a scientist has to perfuse one mouse at a time, and (iii) it requires additional equipment and training before a scientist can insert a cannula to perfuse the liver. LSEC isolation becomes even more challenging in mice with liver pathologies

A full list of affiliations appears at the end of the paper. ✉ e-mail: [mahak.singhal@medma.uni-heidelberg.de](mailto:mahak.singhal@medma.uni-heidelberg.de)

including fibrosis and cancer. The accumulation of excessive extracellular matrix requires longer perfusion times with digestion mix<sup>9</sup>.

To tackle these challenges and isolate LSECs in high purity, the present study describes a perfusion-independent protocol for LSEC isolation. By opting for a perfusion-independent procedure, we circumvented the need for specialized equipment and training as well as substantially improved the scale of LSEC isolation. Focusing on the first step of the procedure – the digestion of the liver tissue, we found that intermittent mixing of tissue suspension with a serological pipette, instead of a syringe-needle combination, safeguarded LSECs and enabled a yield that is comparable or higher to previously reported yields from perfusion-dependent isolation protocols<sup>8</sup>. Further characterization revealed that our isolation procedure led to a uniform capturing of LSECs from all zones of the hepatic sinusoid, allowing for zone-specific LSEC isolations. Together, the newly established LSEC isolation protocol enables life scientists to study liver vasculature with minimal prior knowledge and training and propels further research efforts in understanding LSEC biology.

## Results

### Step-by-step procedure for isolating liver sinusoidal endothelial cells

The whole procedure can be classified into three major steps (Fig. 1):

- (i) Liver tissue processing to obtain single-cell suspension (~45 min)
- (ii) Enrichment of non-parenchymal cells (~30 min)
- (iii) Isolation of high-purity LSECs (~40–60 min)

The time required for the isolation depends on the number of mice processed in parallel as well as the total cells sorted via FACS. Additionally, it would rely on FACS settings used for cell sorting. FACS sorting with a 70 μm nozzle allows for high-speed analysis with up to

15,000 events processed per second, while a 100 μm nozzle would allow cell sorting with a speed of up to 10,000 events per second. The selection of FACS settings would largely depend on the downstream application of isolated LSECs. The time indicated here is based on processing four mice in parallel and isolating 1 million LSECs for gene expression analysis.

#### Step I—liver tissue processing.

1. Before sacrificing the mice, freshly prepare the digestion buffer and store it at 4 °C till use.  
5 ml of digestion buffer is required to digest one adult mouse liver, approximately weighing 1 g.
2. Excise the liver and transfer it into a 6 cm petri dish containing phosphate buffered saline (PBS) solution.
3. Swiftly wash the liver in the PBS solution and transfer it to the dry lid for chopping.
4. Use curved scissors to fine chop the liver as shown in Fig. 1.  
Coarse chopping the mouse liver tissue into small fragments will result in comparable yield of LSECs as finely chopped tissue (Fig. 2c). However, it may affect intermediate steps involving 100 μm cell strainer and occasionally clog the LS column.
5. Transfer the minced liver into a 15 ml conical tube and add 5 ml of the digestion buffer.
6. Incubate the samples at 37 °C in a pre-heated incubation shaker at 180 rotations per minute for 30 min.
7. During the digestion, perform intermittent mixing of samples with a 10 ml serological pipette every 10 min for a total of three times.  
This protocol was optimized using 10 ml serological pipettes with an opening mouth diameter of roughly 1.2 mm. Using a serological

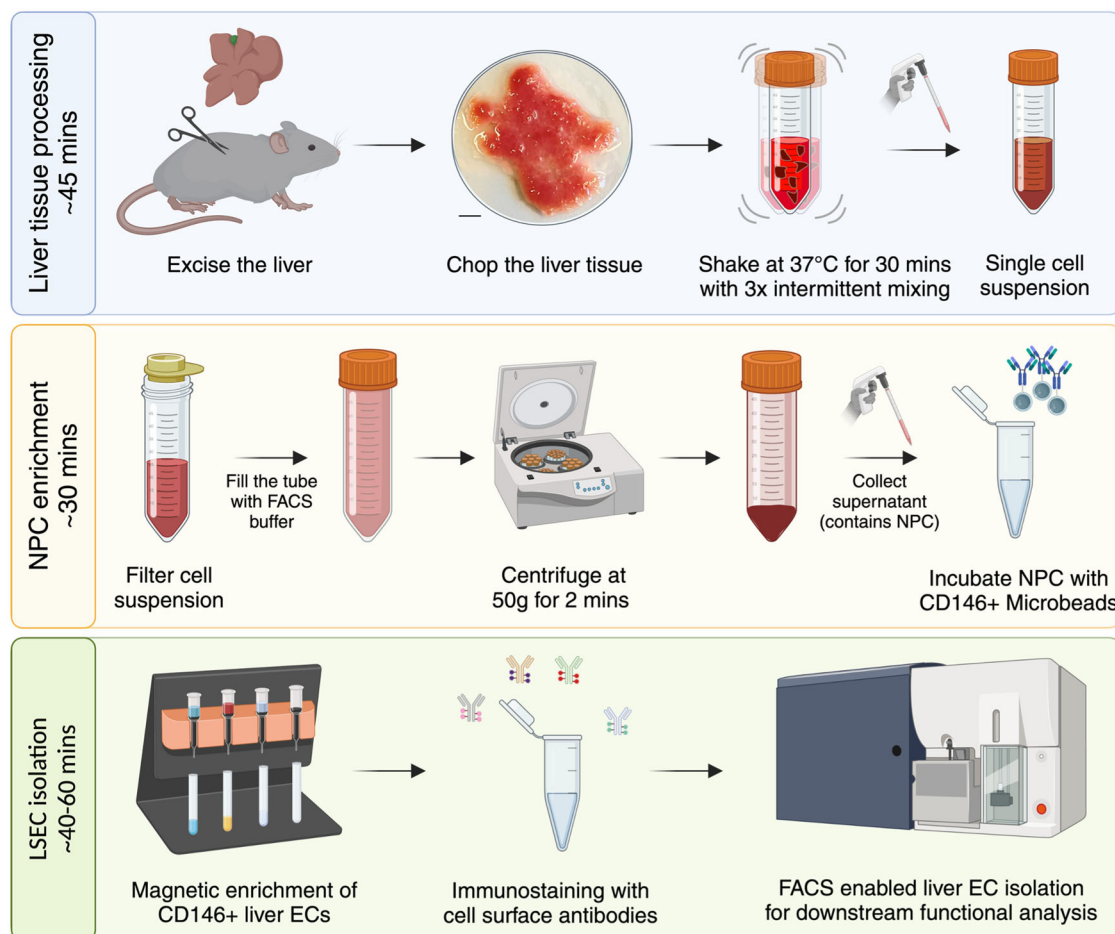
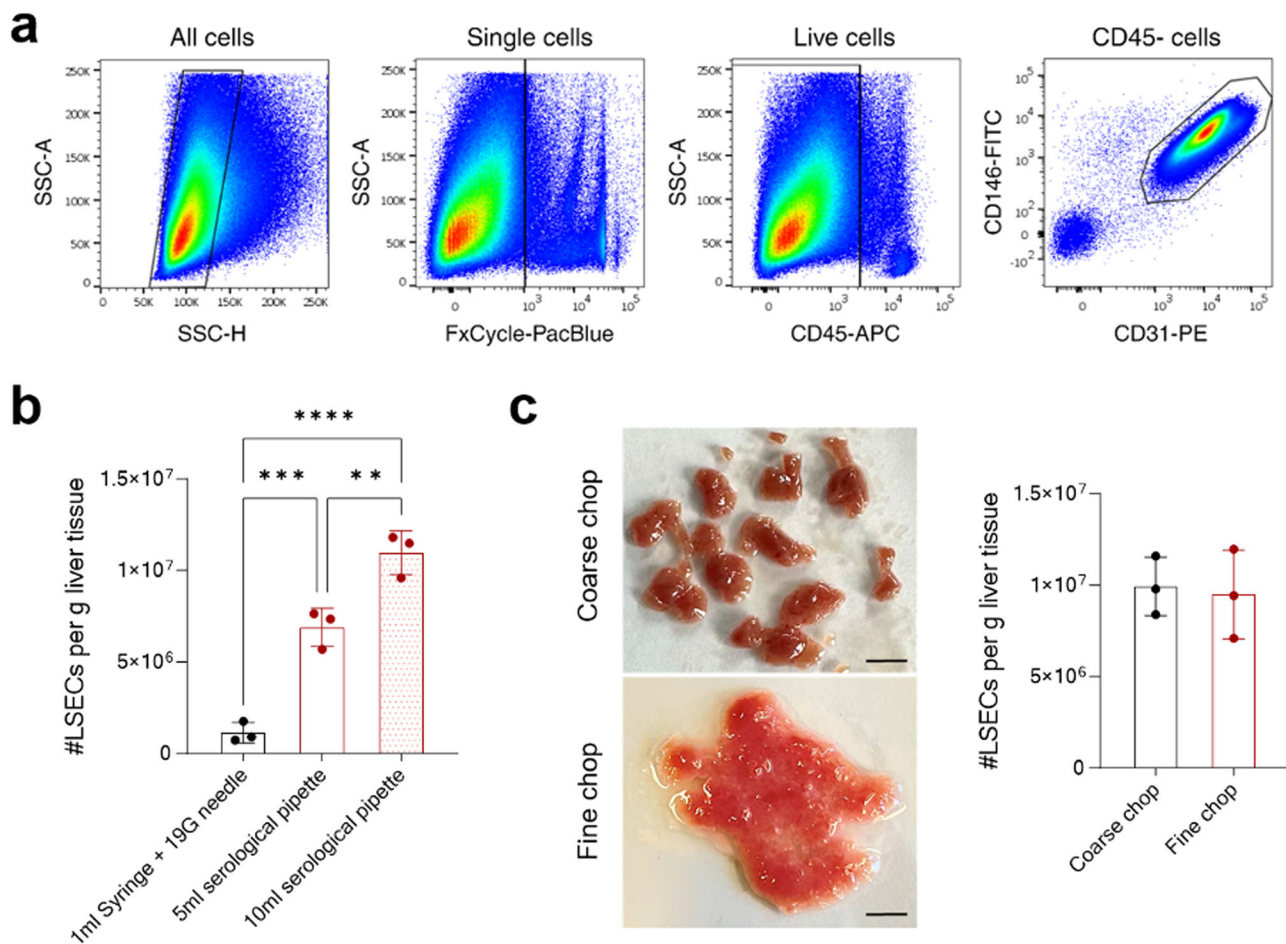


Fig. 1 | Step-by-step schematic depiction of the LSEC isolation protocol. Scale bar = 5 mm.



**Fig. 2 | Optimizing the tissue digestion step of LSEC isolation.** **a** Sequential FACS gating strategy to identify and sort LSECs. **b** The dot plot shows FACS-based (using CountBright plus counting beads) counting of LSECs retrieved using different methods for intermittent mixing during tissue digestion. [mean  $\pm$  SD,  $n = 3$  mice].  $**P < 0.01$ ,  $***P < 0.001$  and  $****P < 0.0001$  (one-way ANOVA test). **c** The liver

tissue was either coarsely or finely chopped and used to isolate LSECs. On the left, images of differently chopped liver tissues are shown. Scale bar = 5 mm. On the right, the dot plot shows the total count of LSECs isolated from differently chopped liver tissues [mean  $\pm$  SD,  $n = 3$  mice].

pipette with a different opening diameter might affect the quality of cell suspension and the overall LSEC yield.

After 30 min of digestion, there might still be remaining liver fragments, yet proceed with the next step. Elongating the digestion step might negatively affect the health of isolated LSECs.

#### Step II – enrichment of non-parenchymal cells (NPCs).

8. Transfer the digested cell suspension with a 10 ml serological pipette into a 50 ml conical tube through a 100  $\mu$ m cell strainer.
9. In the case of a blocked cell strainer, use the plunger of a 5 ml syringe to press the remaining liver pieces through the cell strainer.
10. Wash the plunger and the cell strainer with 5 ml of FACS buffer.
11. Fill the conical tube with FACS buffer up to the mark of 50 ml.
12. Centrifuge the tube at 50 g, 4  $^{\circ}$ C for 2 min.
13. The pellet primarily contains hepatocytes, while the supernatant is enriched for NPCs. Carefully transfer the supernatant into a new 50 ml conical tube.
14. Centrifuge the tube at 450 g, 4  $^{\circ}$ C for 5 min and discard the supernatant.
15. The resulting pellet consists of NPCs. Resuspend the pellet in 200  $\mu$ l of CD146-selection buffer and incubate at 4  $^{\circ}$ C for 20 min.
16. During the incubation time, prepare for the magnetic enrichment.
  - a. Place the LS columns in the QuadroMACS<sup>TM</sup> magnetic separator rack.
  - b. Equilibrate each column by adding 5 ml of FACS buffer.

#### Step III – isolation of high-purity LSECs.

17. Wash the cells with 5 ml of FACS buffer and centrifuge at 450 g, 4  $^{\circ}$ C for 5 min. Subsequently, discard the supernatant.
18. Resuspend the NPC pellet in 1 ml of FACS buffer and apply it to an equilibrated LS column through a 100  $\mu$ m cell strainer.
19. Wash the filter with 1 ml of FACS buffer.
20. Allow the NPC suspension to pass through the LS column.
21. Wash the LS column by applying 9 ml of FACS buffer.
22. Remove the LS column from the magnet and place it onto a fresh 15 ml conical tube.
23. Add 5 ml of FACS buffer to the LS column. Elute the cells by purging the column with the supplied plunger.
24. Centrifuge the elute at 450 g, 4  $^{\circ}$ C for 5 min and discard the supernatant.
25. Resuspend the pellet in 200  $\mu$ l of the staining mix and transfer it to a 1.5 ml tube.
26. Incubate the cell suspension at 4  $^{\circ}$ C for 20 min, protected from the light.
27. Wash the cells with 1 ml of FACS buffer and centrifuge at 450 g, 4  $^{\circ}$ C for 5 min.
28. Carefully remove the supernatant and resuspend the pellet in 200  $\mu$ l of FACS buffer.
29. Transfer the sample into a FACS tube through the 35  $\mu$ m cell strainer in the lid.

30. Store filtered samples in FACS tubes on ice and proceed with FACS-based cell sorting.
  - a. Before analyzing a sample, add dead cell exclusion dye (FxCycle violet stain, 1  $\mu$ l per sample).
  - b. Sort viable CD31+CD146+ cells using the FACS gating strategy shown in Fig. 2a.
  - c. Reanalyze a small portion of FACS-sorted LSECs to evaluate the purity of sorted cells.
  - d. Depending on the downstream application, process the FACS-sorted LSECs.

We recommend plotting a histogram of CD117/Kit as a control for successful isolation of LSECs from all regions of a hepatic sinusoid. A successful LSEC isolation will result in a plateau-like distribution in the histogram for CD117 staining. Refer to the Fig. 5a.

### Optimization of the liver tissue digestion procedure

Focusing on the tissue digestion step of the LSEC isolation procedure, we first compared different ways of intermittent mixing during incubation with the digestion mix. Here, a 19 G needle—1 ml syringe combination was compared to a serological pipette (5 ml, mouth diameter 2.5 mm or 10 ml, mouth diameter 1.2 mm) for mixing the tissue slurry. Unexpectedly, serological pipette-mediated mixing safeguarded the integrity of LSECs and resulted in a far higher yield of LSECs as compared to needle-syringe mediated mixing (Fig. 2b). Among serological pipettes, the use of a 10 ml pipette for mixing led to a lower chance of remaining tissue fragments after digestion on the cell strainer and a more uniform cell suspension as compared to 5 ml pipette. Subsequently, liver tissues digested with a 10 ml pipette resulted in a significantly higher number of LSECs over a 5 ml pipette (Fig. 2b).

Next, we employed different grades of chopping of the liver tissues, comparing coarsely and finely chopped liver tissue for LSEC isolation (Fig. 2c). Surprisingly, no major difference was observed in the final yield of retrieved LSECs from either of the compared chopping methods (Fig. 2c). However, coarsely chopped tissue often required additional effort while processing different downstream steps of the protocol. First, coarsely chopped tissue often led to incomplete tissue digestion and accumulation of leftover fragments on the cell strainer. Second, we observed a higher frequency of clogging in LS columns when enriching LSECs from coarsely chopped liver tissues. Together, these experiments suggest that finely chopped liver tissue processed with a 10 ml serological pipette offers an optimal way to digest the liver tissue for isolating LSECs.

### Isolating LSECs from different lobes of the mouse liver

Employing the above-described perfusion-independent procedure, we reliably isolated an average of  $10 \times 10^6$  LSECs per 1 g of the mouse liver (Fig. 2b, c). The isolated liver endothelial cells were also positively stained for additional sinusoidal markers, such as Stabilin-2 and Lyve-1 (Fig. S1a), validating their LSEC identity. Next, we compared whether our protocol could uniformly isolate LSECs from all lobes of the liver tissue. To this end, the liver tissue was segregated into three parts—left lobe, median lobes, and right lobes, each constituting nearly one-third of the total liver mass (Fig. S1b). After that, LSECs were isolated from each of these liver parts using our protocol. We could successfully isolate LSECs from all three parts of the liver, with a yield of nearly  $4 \times 10^6$  LSECs from each of the segregated liver parts (Fig. S1b). Given that we could isolate a similar number of LSECs from three regions of the liver that weigh roughly the same suggests a broad application of the protocol to preclinical surgical experiments where often only some part of the liver is accessible for downstream analytical experiments. A particular application would be two-third partial hepatectomy, which represents one of the well-studied tissue regeneration models<sup>10,11</sup>. Our method will allow scientists to isolate LSECs from the resected lobe of the liver during hepatectomy and compare them with LSECs isolated from the regenerated lobes in an indexed manner. This is often not possible with current perfusion-dependent LSEC isolation methods. This would substantially

improve the robustness of lineage tracing experiments, where currently such indexed analyses are often not possible.

### Extracting LSECs from fibrotic mouse liver

Next, we questioned whether our method could be applied for isolating LSECs from fibrotic liver tissues. Accumulation of the extracellular matrix presents a technical hurdle in digesting the tissue and current perfusion-dependent isolation methods often have limited efficacy. To this end, we employed a diet-based preclinical model of metabolic dysfunction-associated steatohepatitis (MASH)<sup>12</sup>. Mice were fed with either standard or Choline deficient L-amino acid defined (CDAA) diet for 10 weeks to induce MASH as demonstrated by hepatocyte ballooning and accumulation of extracellular matrix in liver tissues (Fig. 3a). Using our method, we successfully isolated LSECs from fibrotic liver tissues (Fig. 3b). Further, quantitative PCR analysis revealed that LSECs from fibrotic livers have reduced expression of sinusoidal marker genes, such as *Stab1*, *Stab2*, and *Fcgrb*, as compared to LSECs isolated from healthy livers (Fig. 3c), suggesting the loss of sinusoidal characteristics of LSECs during fibrosis.

### Obtaining LSECs from pig liver tissues

To test the wider applicability of our method for isolating LSECs from the liver tissue of higher vertebrate species, we collected fresh liver samples from Landrace pigs. Processing pig liver tissues posed specific technical challenges due to the non-availability of magnetic beads for positive selection and the limited availability of fluorescence-conjugated anti-pig antibodies for FACS-based enrichment. Hence, we relied only on FACS-based cell isolation with CD31 as a primary antigen to sort pig liver ECs (Fig. 3d) and managed to retrieve CD31+ LSECs in high numbers (Fig. 3e). Downstream quantitative PCR analysis illustrated the high purity of our isolated CD31+ LSECs as they manifested multi-log fold higher expression of the key endothelial genes as compared to CD31− cells (Fig. 3f). Relying on our isolation from pig liver tissues, we envision a broad application of our perfusion-independent protocol for isolating LSECs from small biopsies and limitedly available human liver tissues.

### Establishing the primary culture of enriched LSECs

To broaden the downstream application of our LSEC isolation method, we investigated whether LSECs can be cultured for downstream ex vivo analyses. To this end, LSECs were enriched using the CD146-selection magnetic beads and then placed in a culture dish. Intriguingly, the majority of LSECs adhered to the Petri dish, suggesting the high viability of isolated LSECs. Next, we systematically characterized primary LSEC cultures. Here, we first stained primary LSEC cultures with endothelial cell-specific marker ERG and quantitated the percentage of endothelial cells among all DAPI-positive cells (Fig. 4a). The majority (>98%) of adhered cells were stained positively for ERG, validating the purity of the established LSEC cultures. Additionally, we stained primary cultures for cell-specific markers—CD31 (an endothelial cell-specific), Desmin (a stellate cell-specific), and F4/80 (a macrophage-specific). These analyses suggested that non-endothelial cells in LSEC cultures are macrophages and stellate cells (Fig. S2). Secondly, we characterized primary LSEC cultures for the markers of sinusoidal endothelium—Stabilin-2 and CD32b. Immunofluorescence (IF) staining revealed that the majority of cultured endothelial cells are concurrently positive for Stabilin-2 and CD32b (Fig. 4b, c). These analyses complement the FACS analysis of isolated LSECs, which were similarly found positive for Stabilin-2 expression (Fig. S1a). Thirdly, we pursued scanning electron microscopy to visualize fenestrations in the adhered LSECs. The presence of nanosized pores across imaged endothelial cells unambiguously suggests that adhered cells are bona fide LSECs (Fig. 4d). Overall, these data characterize the sinusoidal characteristics of primary cultures of LSECs established after perfusion-independent digestion of liver tissues.

### Retrieving LSECs from different zones of the hepatic sinusoid

Considering LSECs constitute a rather heterogeneous cell population with their function displaying a zonation along the hepatic sinusoid, we next

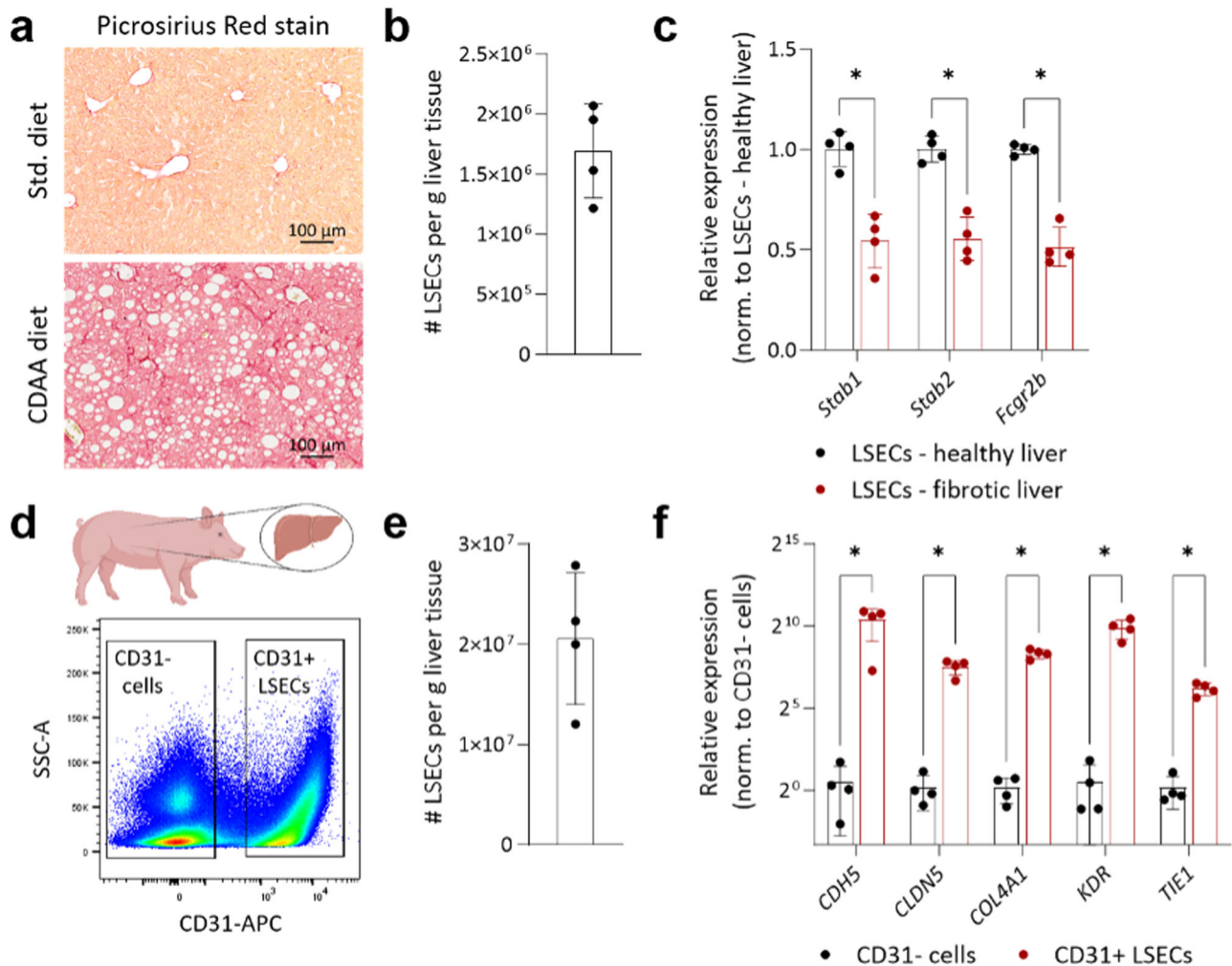


**Fig. 3 | Isolating LSECs from fibrotic mouse and steady-state pig liver tissues.** a–c Mice were fed with a standard or CDAA diet for 10 weeks. a Images show Picrosirius Red staining on the liver sections. LSECs were isolated from healthy and fibrotic liver tissues. Scale bar = 100  $\mu$ m. b The dot plot shows the number of LSECs isolated from fibrotic mouse liver. [mean  $\pm$  SD,  $n = 4$  mice]. c Quantitative PCR analyses to compare the expression level of various sinusoidal genes in LSECs isolated from either healthy or fibrotic mouse liver tissues. [mean  $\pm$  SD,  $n = 4$  mice].

\* $P < 0.05$  (Mann–Whitney test). d–f Liver tissues collected from healthy pigs were processed to isolate LSECs. d FACS plot showing gating strategy to isolate CD31+ LSECs and CD31– cells. e The dot plot shows the number of LSECs isolated from pig liver tissues. [mean  $\pm$  SD,  $n = 4$  pigs]. f Quantitative PCR analyses to compare expression of various vascular genes between CD31+ LSECs and CD31– cells. [mean  $\pm$  SD,  $n = 4$  pigs]. \* $P < 0.05$  (Mann–Whitney test).

wanted to investigate whether our protocol is capturing LSECs from all different regions of the hepatic sinusoid. To achieve this, CD31+CD146+ LSECs were sequentially analyzed for the surface abundance of CD117 (*Kit*). In line with previous publication<sup>13</sup>, CD117 staining on LSECs manifested a plateau-like shape (Fig. 5a), suggesting that our protocol was able to capture LSECs from all zones of the hepatic sinusoid. To verify the spatial origin of LSECs, we stratified and isolated LSECs based on the mean fluorescence intensity of CD117—periportal (PP, CD117<sup>low</sup>), midlobular (MD, CD117<sup>med</sup>), and pericentral (PC, CD117<sup>high</sup>). Gene expression analyses corroborated the origin of sorted LSECs with periportal LSECs enriched for *Dll4*, *Efnb2*, *Il1a*, and *Sox17* whereas pericentral LSECs enriched for *Dkk3*, *Kit*, *Thbd*, and *Wnt9b* (Fig. 5b). These data substantiate that our protocol can successfully capture LSECs from all zones of the hepatic sinusoid and present a strategy for isolating zone-specific LSECs for downstream functional analyses.

### Simultaneous isolation of LSECs and Kupffer cells

To assess whether the NPC fraction after perfusion-independent tissue digestion also consists of Kupffer cells, we analyzed the NPC fraction for CD45 and F4/80 with flow cytometry. A clear Kupffer cell (CD31–CD45+F4/80+) population was identified within the NPC fraction (Fig. S3a). Quantification with FACS counting beads estimated that an

average of  $1.5 \times 10^6$  Kupffer cells and  $1.1 \times 10^7$  LSECs can be simultaneously retrieved per 1 g of the mouse liver (Fig. S3b).

### Discussion

Revisiting every step of the liver sinusoidal endothelial cell isolation procedure, the present study established a perfusion-independent high-throughput method to isolate ultrapure LSECs from the mouse liver. Combining our newly established liver digestion procedure with magnetic and FACS-based purification steps, ultrapure (>98%) LSECs were retrieved in a yield far higher than existing perfusion-independent methods and a comparable yield to existing perfusion-dependent methods. Circumventing the need for perfusion means that the current protocol (i) offers scalability, allowing researchers to perform parallel isolation of LSECs from relatively large cohorts of mice, (ii) bypasses the need for substantial hands-on training to insert a cannula for perfusing the liver, and (iii) minimizes the alterations in molecular circuits of isolated LSECs driven by perfusion-induced shear stress.

### Tissue processing

Focusing particularly on the liver digestion step, we optimized the protocol to maximize tissue digestion along with safeguarding the health and

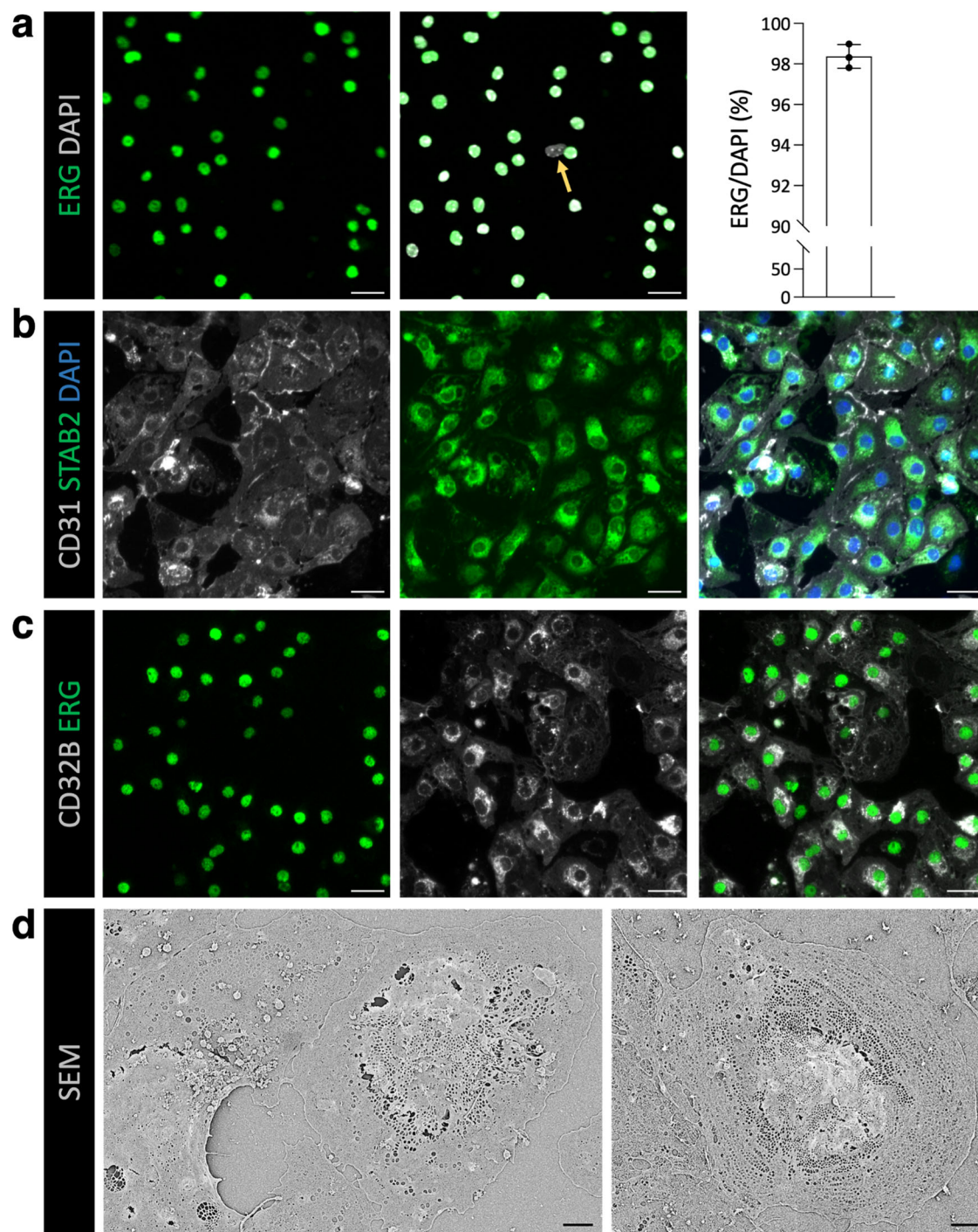


**Fig. 4 | Characterizing the primary cultures of isolated LSECs.** **a–d** LSECs were isolated using perfusion independent digestion method, followed by positive selection using CD146-magnetic beads. After that, enriched LSECs were placed in culture. **a** Primary LSEC cultures were stained for an endothelial cell marker (ERG, in green) and nuclear marker (DAPI, in gray). On the left, images show IF-stained LSEC cultures. Scale bar = 25  $\mu$ m. The yellow arrow highlights an ERG-negative cell.

On the right, the dot plot shows the percentage of ERG-positive cells of DAPI-positive cells. [mean  $\pm$  SD,  $n = 3$  wells]. **b** Images show IF-stained LSECs with CD31 (in gray), Stabilin-2 (in green), and DAPI (in blue). Scale bar = 25  $\mu$ m. **c** Images show IF-stained LSECs with CD32b (in gray) and ERG (in green). Scale bar = 25  $\mu$ m. **d** Representative scanning electron microscopy images of cultured LSECs. Scale bar = 2  $\mu$ m.

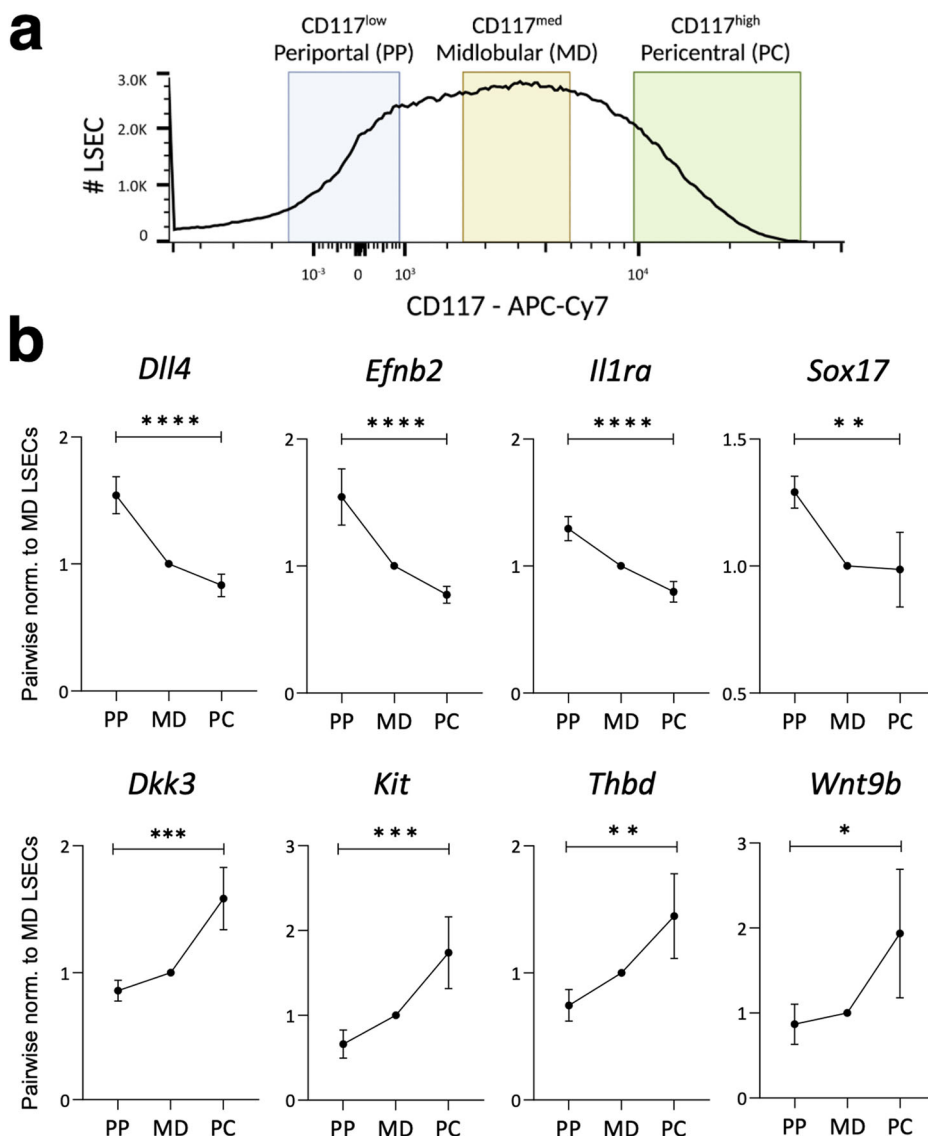
integrity of LSECs. Surprisingly, use of serological pipettes instead of a needle-syringe based intermittent mixing of tissue digestion mix was important to prevent the loss of LSECs and obtain uniform results. Potentially, mixing with serological pipette reduced mechanical stress caused by syringe-needle combination, thereby preserving LSEC health. Furthermore, fine chopping of liver tissue led to smooth processing and a high recovery of viable LSECs. These two alterations in the processing of

liver tissues yielded a nearly 5-fold higher number of LSECs as compared to previous perfusion-independent isolation approaches<sup>14</sup>.

#### Digestion buffer

In the present study, we used research-grade liberase enzyme for digesting the liver tissue. This was primarily driven by the user experience as liberase offered very high consistency in terms of tissue digestion among various

**Fig. 5 | Isolation and validation of isolated zone-specific LSECs. a, b** LSECs were isolated from different regions of a liver sinusoid. **a** CD117-based stratification to undertake hepatic zone-specific LSEC isolation. **b** Gene expression analysis for known periportal (top) and pericentral (bottom) zone-specific LSEC genes [mean  $\pm$  SD,  $n = 4$  mice]. \* $P < 0.05$ , \*\* $P < 0.01$ , \*\*\* $P < 0.001$  and \*\*\*\* $P < 0.0001$  (one-way ANOVA test).



production lots. In contrast, the efficacy of collagenase and dispase varied depending on their lots, often requiring different concentrations of the enzymes to be used for tissue processing. Yet, all collagenase-based enzymatic digestion mixtures should work with the current protocol. We have recommended the liberase-based digestion buffer largely due to our own experiences.

### Isolating other hepatic cells

While the present study focused on optimizing the isolation of LSECs from the liver tissue, we can envision a rather broad application of the current protocol for the isolation of various hepatic cells. For example, in the step with a 50 g centrifugation during NPC enrichment, the cell pellet largely consists of hepatocytes and can potentially be used for various hepatocyte-based assays. Likewise, the total NPC fraction can be used to isolate tissue infiltrating immune cells and hepatic stellate cells. While immune cells can be purified employing either cell-specific surface markers for FACS or selective adhesion for Kupffer cells<sup>15,16</sup>, NPCs can be processed through a Nycodenz gradient to enrich stellate cells as described previously<sup>9</sup>. In line, we observed Kupffer cells, marked by CD45+F4/80+ population, in our NPC fraction, which could potentially be sorted for further downstream analyses, hence allowing for simultaneous analysis of LSECs and Kupffer cells from the same liver sample. The yield of Kupffer cells in our perfusion-independent method was

consistent with a recent publication describing a perfusion-based method to isolate liver macrophages<sup>15</sup>. Together, by achieving uniform digestion of the liver tissue in a perfusion-independent manner, we believe that we overcame the critical bottleneck, and our established protocol can be applied to potentially isolate all hepatic cell types.

### Broad applicability for LSEC isolation

Beyond establishing LSEC isolation from healthy mouse livers, we tested our method to obtain viable LSECs from livers where perfusion is often not possible. We demonstrate that our method efficiently retrieved LSECs from surgically resected individual lobes of the liver as well as fibrotic livers derived from MASH mice. Intriguingly, the high efficiency and purity of LSECs isolated from pig liver tissues showcase the robustness of our method for investigating LSECs from liver specimens derived from higher vertebrates and even limited clinical human material.

### Primary cultures of LSECs

The successful realization of primary cultures of isolated LSECs with sinusoidal characteristics makes it possible to undertake a wide array of in vitro mechanistic assays to study organotypic molecular mechanisms in the liver vasculature. In our experience, dual sorted (MACS enrichment followed by FACS) LSECs were viable but failed to properly adhere to culture dishes. Hence, we opted to culture MACS-enriched LSECs, which

consistently resulted in >98% purity and robust sinusoidal characteristics as marked by traditional LSEC makers, such as Stab2 and CD32b and visualized by fenestrations, a key hallmark of LSEC morphology. Our data suggest that magnetic enrichment alone is sufficient to establish primary cultures, while dual sorting with magnetic enrichment and FACS is more suitable for highly sensitive downstream assays, such as RNAseq and proteomics, which require a very high purity of LSECs.

### Zone-specific LSEC isolation

Addressing the functional heterogeneity in LSECs across the hepatic sinusoid, we tested the surface presentation of CD117 (Kit) among CD31+CD146+ LSECs. Indeed, our isolation protocol successfully captured LSECs from all regions of the hepatic sinusoid as demonstrated by the expected trend of the expression of periportal and pericentral LSEC-specific genes. These periportal and pericentral marker genes were selected based on published single-cell RNA sequencing study of the liver vasculature<sup>17</sup>. Building on these findings, our method can be employed to isolate hepatic zone-specific LSECs in high quantities. In our analysis, we stratified LSECs based on the mean fluorescence intensity of CD117. Based on this parameter, the lowest 15% of LSECs were sorted as CD117<sup>low</sup>, and the highest 15% of LSECs were categorized as CD117<sup>high</sup>. This would imply that quantitatively, we could isolate around 1.5 million LSECs each from the periportal and pericentral regions of the hepatic sinusoid. The high quantity of LSECs isolated from different hepatic zones will empower future studies to undertake functional analyses such as proteomics and even observe post-translational modifications in zoned homeostatic LSECs.

In conclusion, the method described in the present study should facilitate high-throughput isolation of ultrapure LSECs. The perfusion-independent nature of the procedure should ensure high reproducibility of experiments and favor a broad application of the isolation method in laboratories that classically have little liver expertise. The current experiments demonstrate our continuous efforts to simplify the isolation protocol for different hepatic cells to better understand cellular and molecular crosstalk within the liver microenvironment.

## Materials and methods

### Mice and pig tissues

C57BL/6NRj (aged 8–10 weeks) mice were procured from Janvier Laboratories. All mice were housed on a 12-h light/12-h dark cycle with free access to food and drinking water in specific pathogen-free animal facilities. Liver tissues from Landrace pigs were kindly provided by Prof. Constanze Schmidt, University Hospital Heidelberg, Heidelberg University, Heidelberg, Germany (ethics vote—T-19/24). All animal experiments were per the governmental (Regierungspräsidium Karlsruhe, Germany) and institutional (Heidelberg University, Mannheim, Germany) guidelines for the care and ethical use of laboratory animals.

### Liver tissue digestion and subsequent enrichment of LSECs

C57BL/6NRj mice were euthanized by cervical dislocation, and liver tissues were excised for isolating LSECs. The step-by-step method for isolating LSECs is described in the results section. Here, we describe all materials used and the composition of various buffers.

Chopped liver tissue from each mouse were digested in 5 ml liberase-based digestion mix (5 ml of DMEM [Thermo Fisher Scientific, Cat #61965059] + 1 mg Liberase<sup>TM</sup> Research Grade [Roche, Cat #5401127001] + 0.1 mg DNase I [Sigma-Aldrich, Cat #10104159001]).

For magnetic enrichment of LSECs, NPCs from each liver were incubated in 200 µl of CD146-selection mix (175 µl FACS buffer + 25 µl of CD146 microbeads [Milentyi Biotec, Cat #130-092-007]). FACS buffer used for preparing the selection mix and washing the LS columns [Milentyi Biotec, Cat #130-042-401] contains 3% FCS in PBS solution.

For pig liver samples, digested single cell suspension was directly stained with APC-conjugated anti-pig CD31 [BioRad, Cat #MCA1746APC] antibody.

### Preclinical MASH model

MASH was induced in mice by feeding *ad libitum* with either a standard diet [Ssniff, Cat #V1534-000] or CDAA diet [Ssniff, Cat #E15666-94] for 10 weeks as previously described<sup>18</sup>. Liver tissue sections were analyzed with Picrosirius red staining to evaluate liver fibrosis as previously described<sup>14</sup>.

### Flow cytometry-based analysis and sorting

Enriched NPC or MACS-enriched LSECs were stained for various surface markers, using antibodies listed in the following table. Dead cells were excluded by FxCycle Violet staining [Thermo Fisher Scientific, Cat #F10347]. Stained cells were analyzed on either BD FACS Melody<sup>TM</sup> or BD Aria II cell sorting platforms. Total LSECs per liver were calculated using CountBright plus counting beads [Thermo Fisher Scientific, Cat #C36995]. FACS data were analyzed using FlowJo software.

Antigen	Host	Reactivity	Fluorophore	Clone	Supplier	Cat. No.
CD31	rat	mouse	PE	MEC13.3	BioLegend	102508
CD31	rat	mouse	APC	MEC13.3	BioLegend	102510
CD146	rat	mouse	FITC	ME9F1	BioLegend	134706
CD146	rat	mouse	PE	ME9F1	BioLegend	134706
CD117	rat	mouse	APC-Cy7	2B8	BioLegend	105826
Lyve1	rat	mouse	AF488	ALY7	Thermo Fisher Scientific	53-0443-82
F4/80	rat	mouse	PE	BM8	BioLegend	123110
CD45	rat	mouse	FITC	30-F11	BioLegend	103108
CD45	rat	mouse	APC	30-F11	BioLegend	103112
CD45	rat	mouse	APC-Cy7	30-F11	BioLegend	103116
CD31	mouse	pig	APC	LCI-4	BioRad	MCA1746APC
Stab2	rabbit	mouse	FITC	polyclonal	Bioss Antibodies	BS-12346R-FITC

### Immunofluorescence staining on cultured LSECs

96-well dishes were coated with Fibronectin [Merck Millipore, Cat #341631]. 300,000 CD146-enriched LSECs were thereupon added to each well and cultured at 37 °C and 5% CO<sub>2</sub> for 16 h in complete mouse endothelial cell medium [Pelo Biotech, Cat #PB-M1168]. Cells were subsequently washed with PBS, fixed in 4% PFA [Carl Roth, Cat #0335.1], blocked with 10% normal donkey serum [Biozol, Cat #LIN-END9010-10] and incubated in a primary antibody mix consisting of different combinations of goat anti-mouse CD31 [R&D Systems, Cat #AF3628], goat anti-mouse CD32b [R&D Systems, Cat #AF1460], rabbit anti-mouse Desmin [Abcam, Cat #ab15200], rabbit anti-mouse ERG [Abcam, Cat #ab196149], rat anti-mouse F4/80 [BioLegend, # 123102], and rabbit anti-mouse Stabilin-2 antibodies overnight. Ensuing washing in PBS, cells were incubated with a mix composed of DAPI [Invitrogen, Cat #D1306], AF488-conjugated donkey anti-goat [Thermo Fisher Scientific, Catalog # A-11055], AF647-conjugated donkey anti-rabbit [Thermo Fisher Scientific, Cat #A-31573], AF555-conjugated donkey anti-goat [Thermo Fisher Scientific, Cat #A-32816], and AF488-conjugated donkey anti-rat [Thermo Fisher Scientific, Cat #A-21208] secondary antibodies at room temperature and mounted using Dako mounting medium [Agilent, Cat #S302380-2]. Stained cells were imaged with Leica Thunder Imaging platform and images were analyzed with Fiji. Stabilin-2 antibody was generated in-house and characterized previously for tissue and cellular stainings<sup>19</sup>.

### Scanning electron microscopy analysis of cultured LSECs

Glass or plastic coverslips were placed in 12-well plates and coated with Fibronectin [Merck Millipore, Cat #341631]. 3 million CD146-enriched



LSECs were thereupon added to each well and cultured at 37 °C and 5% CO<sub>2</sub> for 16 h in complete mouse endothelial cell medium [Pelo Biotech, Cat #PB-M1168]. Cells were subsequently washed with PBS and fixed with 2.5% glutaraldehyde in 0.1 M PHEM buffer (pH 6.9) at RT for 30 min. They were then washed with PHEM buffer and fixed with 1% osmium tetroxide in PHEM buffer for 30 min on ice. Dehydration was performed in a graded series of acetone for glass coverslips and ethanol for plastic coverslips. The samples were critical point dried using a Leica CPD300 and mounted on SEM aluminum stubs [Plano EM Cat #G301F] using a silver solution [ACHSON 1415—Plano EM Cat #G3692]. The mounted samples were then sputter coated with 5 nm gold palladium [Leica EM ACE600 high vacuum coating system]. The samples were imaged using a Zeiss Leo 1530 SEM with an in-lens detector at a beam energy of 2.0 kV and a working distance of 5 mm.

### Gene expression analysis

Total RNA from 500,000 FACS-sorted LSECs was isolated using PicoPure™ RNA isolation kit [Thermo Fisher Scientific, Cat #KIT0204]. Total RNA was transcribed into complementary DNA using a QuantiTect reverse transcription kit [Qiagen, Cat #205313]. Quantitative PCRs (qPCRs) were performed with TaqMan fast advanced master mix [Thermo Fisher Scientific, Cat #4444557]. TaqMan primers (*Actb*, Mm00607939\_s1; *ACTB*, Ss03376563\_uH; *CDH5*, Ss03378336\_u1; *CLDN5*, Ss03373518\_u1; *COL4A1*, Ss06915326\_mH; *Dll4*, Mm00444619\_m1; *Dkk3*, Mm00443800\_m1; *Efnb2*, Mm00438670\_m1; *Fcgr2b*, Mm00438875\_m1; *Illa*, Mm00439620\_m1; *KDR*, Ss03375683\_s1; *Kit*, Mm00445212\_m1; *Sox17*, Mm00488363\_m1; *Stab1*, Mm00460390\_m1; *Stab2*, Mm00454684\_m1; *Thbd*, Mm00437014\_s1; *TIE1*, Ss03373579\_g1; and *Wnt9b*, Mm00457102\_m1) were ordered from Thermo Fisher Scientific. Gene expression was calculated based on the  $\Delta\Delta C_t$  relative quantification method. mRNA abundances were normalized to *Actb/ACTB* expression as indicated.

### Statistics and reproducibility

Statistical analysis was performed using GraphPad Prism version 10 (GraphPad Software). Data are expressed as means  $\pm$  SD. Used statistical tests are indicated in corresponding figure legends. A *P* value of less than 0.05 was considered statistically significant. The sample sizes vary between 3 and 4. The exact sample size for each experiment is included in the figure legend and each data point, if not stated differently in the figure legend, stands for one animal.

### Data availability

The source data for all figures is available in the Supplementary Data file.

Received: 27 August 2024; Accepted: 3 January 2025;

Published online: 08 January 2025

### References

- McConnell, M. J., Kostallari, E., Ibrahim, S. H. & Iwakiri, Y. The evolving role of liver sinusoidal endothelial cells in liver health and disease. *Hepatology* **78**, 649–669 (2023).
- Koch, P. S., Lee, K. H., Goerd, S. & Augustin, H. G. Angiodiversity and organotypic functions of sinusoidal endothelial cells. *Angiogenesis* **24**, 289–310 (2021).
- Augustin, H. G. & Koh, G. Y. Organotypic vasculature: from descriptive heterogeneity to functional pathophysiology. *Science* **357**, eaal2379 (2017).
- Rocha, A. S. et al. The angiocrine factor Rspondin3 is a key determinant of liver zonation. *Cell Rep.* **13**, 1757–1764 (2015).
- Hu, S. et al. Single-cell spatial transcriptomics reveals a dynamic control of metabolic zonation and liver regeneration by endothelial cell Wnt2 and Wnt9b. *Cell Rep. Med.* **3**, 100754 (2022).
- Wang, B., Zhao, L., Fish, M., Logan, C. Y. & Nusse, R. Self-renewing diploid Axin2(+) cells fuel homeostatic renewal of the liver. *Nature* **524**, 180–185 (2015).
- Duan, J. L. et al. Age-related liver endothelial zonation triggers steatohepatitis by inactivating pericentral endothelium-derived C-kit. *Nat. Aging* **3**, 258–274 (2023).
- Meyer, J., Gonelle-Gispert, C., Morel, P. & Buhler, L. Methods for isolation and purification of murine liver sinusoidal endothelial cells: a systematic review. *PLoS ONE* **11**, e0151945 (2016).
- Mederacke, I., Dapito, D. H., Affo, S., Uchinami, H. & Schwabe, R. F. High-yield and high-purity isolation of hepatic stellate cells from normal and fibrotic mouse livers. *Nat. Protoc.* **10**, 305–315 (2015).
- Du, Y. et al. Mouse models of liver parenchyma injuries and regeneration. *Front. Cell Dev. Biol.* **10**, 903740 (2022).
- Michalopoulos, G. K. & Bhushan, B. Liver regeneration: biological and pathological mechanisms and implications. *Nat. Rev. Gastroenterol. Hepatol.* **18**, 40–55 (2021).
- Gallage, S. et al. A researcher's guide to preclinical mouse NASH models. *Nat. Metab.* **4**, 1632–1649 (2022).
- Inverso, D. et al. A spatial vascular transcriptomic, proteomic, and phosphoproteomic atlas unveils an angiocrine Tie-Wnt signaling axis in the liver. *Dev. Cell* **56**, 1677–93 e10 (2021).
- Singhal, M. et al. Endothelial cell fitness dictates the source of regenerating liver vasculature. *J. Exp. Med.* **215**, 2497–2508 (2018).
- Andreato, F. et al. Isolation of mouse Kupffer cells for phenotypic and functional studies. *STAR Protoc.* **2**, 100831 (2021).
- Li, P. Z., Li, J. Z., Li, M., Gong, J. P. & He, K. An efficient method to isolate and culture mouse Kupffer cells. *Immunol. Lett.* **158**, 52–56 (2014).
- Halpern, K. B. et al. Paired-cell sequencing enables spatial gene expression mapping of liver endothelial cells. *Nat. Biotechnol.* **36**, 962–970 (2018).
- Trogisch, F. A. et al. Endothelial cells drive organ fibrosis in mice by inducing expression of the transcription factor SOX9. *Sci. Transl. Med.* **16**, eabq4581 (2024).
- Falkowski, M., Schledzewski, K., Hansen, B. & Goerd, S. Expression of stabilin-2, a novel fasciclin-like hyaluronan receptor protein, in murine sinusoidal endothelia, avascular tissues, and at solid/liquid interfaces. *Histochem. Cell Biol.* **120**, 361–369 (2003).

### Acknowledgements

The authors sincerely thank Dr. Ki Hong Lee for his critical feedback on the manuscript. We thank Dr. Ashik Ahmed Abdul Pari for his help with the generation of figures with [www.BioRender.com](https://www.BioRender.com) (<https://BioRender.com/m71u689>). We are most grateful for the excellent support of the FlowCore and animal facilities of the Medical Faculty Mannheim of Heidelberg University. This work was supported by grants from the Deutsche Forschungsgemeinschaft (DFG) (project A04 to CCW, project B02 to P.S.R.K./S.G., project B03 to C.G., and C06 to M.S. within CRC1366 “Vascular control of organ function” [project number 394046768] and individual grant to M.S. “Investigating the role of endothelial NFKBIZ signaling in tumor progression and metastasis” [project number 510602219]). This study was supported through state funds approved by the State Parliament of Baden-Württemberg for the Innovation Campus Health + Life Science Alliance Heidelberg Mannheim. Y.M. is supported by the scholarship from the China Scholarship Council, China. CS and FW are members of the CRC1550 funded by DFG (project number 464424253). This work was supported by research grants from the German Center for Cardiovascular Research (DZHK) and Else-Kröner Fresenius Foundation to C.S. For the publication fee, we acknowledge financial support by Heidelberg University.

### Author contributions

A.B.E.G., Y.M., T.B., and M.S. conceived and designed the study. A.B.E.G., Y.M., T.B., F.W., L.E., M.W., S.W.K.Z., C.F., R.S., C.G., C.C.W., C.S., S.G., P.S.R.K. and M.S. performed experiments. F.P. and M.H. provided technical support. A.B.E.G., Y.M., T.B., and M.S. analyzed and interpreted data. M.S. supervised the project. A.B.E.G., Y.M., and M.S.

wrote the manuscript. All authors discussed the results and commented on the manuscript.

## Funding

Open Access funding enabled and organized by Projekt DEAL.

## Competing interests

The authors declare no competing interests.

## Additional information

**Supplementary information** The online version contains supplementary material available at <https://doi.org/10.1038/s42003-025-07458-5>.

**Correspondence** and requests for materials should be addressed to Mahak Singhal.

**Peer review information** *Communications Biology* thanks the anonymous reviewers for their contribution to the peer review of this work. Primary Handling Editors: Joao Valente. A peer review file is available.

**Reprints and permissions information** is available at <http://www.nature.com/reprints>

**Publisher's note** Springer Nature remains neutral with regard to jurisdictional claims in published maps and institutional affiliations.

**Open Access** This article is licensed under a Creative Commons Attribution 4.0 International License, which permits use, sharing, adaptation, distribution and reproduction in any medium or format, as long as you give appropriate credit to the original author(s) and the source, provide a link to the Creative Commons licence, and indicate if changes were made. The images or other third party material in this article are included in the article's Creative Commons licence, unless indicated otherwise in a credit line to the material. If material is not included in the article's Creative Commons licence and your intended use is not permitted by statutory regulation or exceeds the permitted use, you will need to obtain permission directly from the copyright holder. To view a copy of this licence, visit <http://creativecommons.org/licenses/by/4.0/>.

© The Author(s) 2025

---

<sup>1</sup>AngioRhythms in Health and Disease, European Center for Angioscience (ECAS), Medical Faculty Mannheim, Heidelberg University, Mannheim, Germany. <sup>2</sup>Faculty of Biosciences, Heidelberg University, Heidelberg, Germany. <sup>3</sup>Medical Faculty Mannheim, Heidelberg University, Mannheim, Germany. <sup>4</sup>Department of Dermatology, Venereology and Allergology, Center of Excellence in Dermatology, University Medical Center and Medical Faculty Mannheim, Heidelberg University, Mannheim, Germany. <sup>5</sup>Angiodiversity and Organ Function, European Center for Angioscience (ECAS), Medical Faculty Mannheim, Heidelberg University, Mannheim, Germany. <sup>6</sup>Department of Cardiology, University Medical Center and Medical Faculty Heidelberg, Heidelberg University, Heidelberg, Germany. <sup>7</sup>DZHK (German Centre for Cardiovascular Research), partner site Heidelberg/Mannheim, Heidelberg University, Heidelberg, Germany. <sup>8</sup>Electron Microscopy Core Facility, Heidelberg University, Heidelberg, Germany. <sup>9</sup>Helmholtz-Institute for Translational AngioCardioScience (HI-TAC) of the Max Delbrück Center for Molecular Medicine in the Helmholtz Association (MDC) at Heidelberg University, Mannheim, Germany. <sup>10</sup>Section of Clinical and Molecular Dermatology, University Medical Center and Medical Faculty Mannheim, Heidelberg University, Mannheim, Germany. <sup>11</sup>Microvascular Heterogeneity, European Center for Angioscience (ECAS), Medical Faculty Mannheim, Heidelberg University, Mannheim, Germany. <sup>12</sup>Ploidy and Organ Physiology, European Center for Angioscience (ECAS), Medical Faculty Mannheim, Heidelberg University, Mannheim, Germany. <sup>13</sup>These authors contributed equally: Anna Babin-Ebell Gonçalves, Yifang Mao, Tinja Baljkas. ✉ e-mail: [mahak.singhal@medma.uni-heidelberg.de](mailto:mahak.singhal@medma.uni-heidelberg.de)